TU Delft

Delft University of Technology

Document Version
Final published version

Licence
CC BY

Citation (APA)
Rotundo, C. D., Sodja, J., & Sinnige, T. (2024). Aeroelastic tailoring of dual-role propellers. In *Aeroelasticity & Structural Dynamics in a Fast Changing World 17 – 21 June 2024, The Hague, The Netherlands* Article IFASD 2024-174

Important note
To cite this publication, please use the final published version (if applicable).
Please check the document version above.

Copyright
In case the licence states “Dutch Copyright Act (Article 25fa)”, this publication was made available Green Open Access via the TU Delft Institutional Repository pursuant to Dutch Copyright Act (Article 25fa, the Taverne amendment). This provision does not affect copyright ownership.
Unless copyright is transferred by contract or statute, it remains with the copyright holder.

Sharing and reuse
Other than for strictly personal use, it is not permitted to download, forward or distribute the text or part of it, without the consent of the author(s) and/or copyright holder(s), unless the work is under an open content license such as Creative Commons.

Takedown policy
Please contact us and provide details if you believe this document breaches copyrights.
We will remove access to the work immediately and investigate your claim.

This work is downloaded from Delft University of Technology.

International Forum on Aeroelasticity and Structural Dynamics
IFASD 2024
17-21 June 2024, The Hague, The Netherlands

AEROELASTIC TAILORING OF DUAL-ROLE PROPELLERS

Carlo Rotundo[1], **Jurij Sodja**[1], **Tomas Sinnige**[1]

[1]Delft University of Technology
Kluyverweg 1, 2629HS Delft, The Netherlands
t.sinnige@tudelft.nl, j.sodja@tudelft.nl

Keywords: Aeroelastic tailoring, composite optimization, dual-role (energy-harvesting) propellers, propeller aerodynamics, static aeroelasticity, structural design

Abstract: An aeroelastic optimization procedure was developed and applied towards the structural blade design for dual-role propellers that are capable of harvesting energy during descent. The purpose of this investigation was to assess the effectiveness of aeroelastic tailoring, when applied towards the improvement of propeller performance for general aviation applications. The optimization objective was to minimize total energy consumption over a climb-cruise-descent mission, with varying cruise distances, as well as constraints on deformations, strains, and laminate feasibility. Results from optimization studies suggest that the ideal flexible constant- and variable- pitch propellers outperformed their rigid counterparts, yielding a decrease in energy consumption in comparison to the referenced rigid variable-pitch propeller by 0.7% – 1.0% and 1.5% – 2.0%, respectively. It has thus been shown that aeroelastic tailoring can yield noticeable improvements in propeller performance by introducing bend-twist and extension-shear coupling to yield an aerodynamic wash-out effect that alleviates blade loads. Coupling the proposed structural optimization framework to a blade aerodynamic geometry optimization procedure is expected to result in further performance enhancements.

NOMENCLATURE

C_P	=	Power coefficient; $C_P = P/(\rho_\infty n^3 D^5)$
C_T	=	Thrust coefficient; $C_T = T/(\rho_\infty n^2 D^4)$
C_d	=	Sectional drag coefficient
C_l	=	Sectional lift coefficient
C_q	=	Sectional torque coefficient
C_t	=	Sectional thrust coefficient
E	=	Mission energy consumption
J	=	Advance ratio; $J = V_\infty/(nD)$
$N_{\text{con, 1}}$	=	Number of inequality constraints
$N_{\text{con, 2}}$	=	Number of equality constraints
N_{obj}	=	Number of mission segments
N_{var}	=	Number of design variables
P	=	Consumed power
P_C	=	Power coefficient; $P_C = C_P\ J^{-3}$
T	=	Propeller thrust
T_C	=	Thrust coefficient; $T_C = C_T\ J^{-2}$
V_{eff}	=	Resultant flow velocity at the blade section
V_∞	=	Resultant freestream flow velocity
f	=	Optimization normalized objective function
g	=	Optimization normalized inequality constraint
h	=	Optimization normalized equality constraint
n	=	Rotation rate of propeller (rev. / s)
$\underline{p}$	=	Blade tip deformation; $\underline{p} = [p_1, p_2, p_3, p_4, p_5, p_6]$
p_{tip}	=	Signed tip displacement; $p_{\text{tip}} = \pm(p_1^2 + p_2^2 + p_3^2)^{1/2}$
r	=	Blade radial position
r_{tip}	=	Blade tip radius
t	=	Time spent in mission (for energy calculation)
$\underline{\Phi}$	=	Normalized design vector
$\underline{\Phi}^{\text{L}}$	=	Normalized lower bound on design vector
$\underline{\Phi}^{\text{U}}$	=	Normalized upper bound on design vector
α	=	Blade sectional angle of attack
β	=	Blade sectional twist angle
ε	=	Normal strain
$\eta_{\text{e.h}}$	=	Energy harvesting efficiency; $\eta_{\text{e.h}} = -8P_C/\pi$
η_{P}	=	Propeller efficiency; $\eta_{\text{P}} = T_C/P_C$
η_{T}	=	Turbine efficiency; $\eta_{\text{T}} = P_C/T_C$
γ_{12}	=	Shear strain
ρ_∞	=	Freestream air density

SCRIPTS

C	:	Compressive value (stresses or strains)	max	:	Maximum value
CP	:	Constant pitch propeller quantity	min	:	Minimum value
T	:	Tensile value (stresses or strains)	rigid	:	Rigid propeller quantity
VP	:	Variable pitch propeller quantity	0.7 or $0.7R$	:	Quantity evaluated at 70% of blade radius

1 INTRODUCTION

Hybrid- or fully electric propeller-based propulsion systems have recently gained interest as an option to reduce greenhouse gas emissions within the rapidly expanding aerospace industry. This focus on electrified propulsion systems has prompted a resurgence in research towards the application of propeller-based propulsion systems. Furthermore, with batteries being used for energy storage and electric motors for supplying power, the electrification of aircraft enables the possibility for energy to be recovered during phases of flight where no power input is required.

The use of aircraft propellers to harvest energy was first suggested by Glauert [1] in 1926, although there was no feasible technology at the time of his research to implement the idea. Over seventy years later, MacCready [2] and Barnes [3–5], revisited the concept through the investigation of a battery-electric and self-launching sailplane, which operates its propellers as energy harvesters during descending flight. Through these efforts, it was observed that introducing the capability of energy-harvesting during descent may enhance range, steepen descent, or add thrust-reversal during landing [2, 5]. Nevertheless, both MacCready and Barnes suggested that the propeller geometry yielding optimal performance during energy-harvesting mode is vastly different from the optimal design for propulsive mode. This is largely attributable to the distinct variations in flow and loading experienced by each blade section between the two scenarios, as exemplified by the inflow conditions and resulting aerodynamic forces depicted in Fig. 1.1.

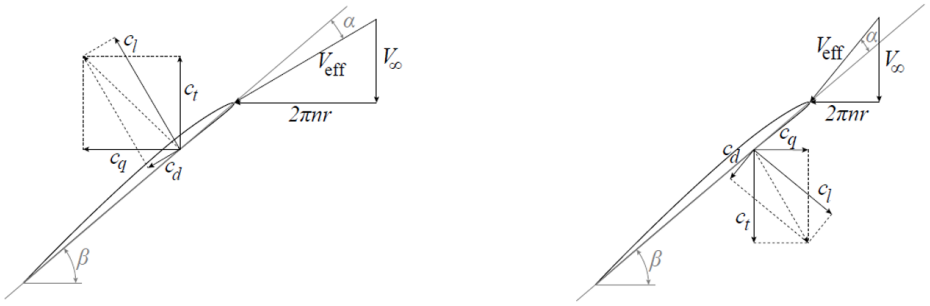

(a) Propulsive operation. (b) Energy-harvesting operation.

Fig. 1.1: Velocity triangles for a propeller operating in propulsive and energy-harvesting modes [6].

Recently, Erzen *et al.* [7] presented a propeller design for exploiting the capability of the *Pipistrel Alpha Electro* for in-flight power recuperation. In this work, the propeller design approach involved considering three disciplines: aerodynamics, electronics, and operations. In particular, the mission profile was designed to exploit the benefits of reverse thrust, including the requirement of a steeper descent. As a result of these efforts, Erzen *et al.* obtained a 19% decrease in energy consumption during the ascend/descend flight pattern and a 27% increase in the number of traffic pattern circuits performed with a propeller that was designed for propulsive and energy-harvesting operation in comparison to a conventional propeller design. These results indicate that considering both propulsive and energy-harvesting operation during the design of propellers has the potential to yield reductions in energy consumption for flight patterns that feature the harvesting of energy during descent. Nevertheless, a more realistic mission should be considered to appropriately estimate differences in energy consumption yielded by each blade design. The performance improvements observed by Erzen *et al.* were heavily dependent on the flight pattern, which was designed to benefit from the use of dual-role propellers.

As shown in Fig. 1.1, the design and operation of dual-role propellers involves considering two opposing load cases: positive thrust and torque during propulsive operation, and negative thrust and torque in energy-harvesting operation. This suggests that a propeller that is designed for

propulsive operation only will underperform in energy harvesting conditions, and vice versa. It was shown by Sinnige *et al.* [6] that a conventional propeller will exhibit a maximum energy harvesting efficiency of approximately 10%, and the blade loading distribution will not resemble that of a typical minimum-induced-loss blade design. This low energy-harvesting performance has been found to be caused by the flow separation and associated viscous losses at the negative angles of attack that the blade sections operate at during this condition [6, 8–10]. An attempt to mitigate this problem has been made during this research through the implementation of a mission-weighted optimization approach that directly accounts for and balances requirements in both the propulsive and energy-harvesting operating conditions. In particular, the novelty of this work concerns the exploitation of blade-axis flexibility through the design of the blade's composite structure using aeroelastic tailoring to minimize total mission energy consumption.

To the best of the authors' knowledge, there has not been any work to-date on the application of aeroelastic tailoring or structural optimization towards the design of dual-role propeller blades, although a considerable amount of research has been published on the design or optimization of flexible propeller or wind turbine blades exclusively for their conventional operating conditions. Aeroelastic tailoring of propeller blades was first studied by Munk [11] who patented the design of wooden blades with diagonal plies yielding favourable deformations as the loading increases. A similar patent application was placed in 2015 by Wood and Ramakrishnan [12] by researchers at General Electric for an open rotor concept with composite blades that deform favourably under increasing load, thereby decreasing noise emissions. In academic contexts, propeller optimization studies aimed at improving efficiency were completed by Dwyer and Rogers [13] Chattopadhyay *et al.* [14] Sandak and Rosen [15], and Sodja *et al.* [16].

Initial flexible propeller design studies focused on applying structural optimization to maximize performance or to reduce deformations. First, Dwyer and Rogers [13] attempted to yield coupling between centrifugal loads and shear forces to maximize on- and off-design performance of a flexible composite propeller. However, they found that the blade mass was too small to yield large enough centrifugal forces to provide a noticeable amount of twist. Through the addition of masses near the blade tip to increase centrifugal loads, Dwyer and Rogers observed an improvement in efficiency of 5% at on-design conditions, and a 20% gain at off-design conditions for a fixed-pitch propeller. Chattopadhyay *et al.* [14] later optimized the design of a prop-rotor for maximum cruise efficiency and hover figure of merit [14]. They did not use structural optimization to improve performance, and instead relied purely on aerodynamic optimization for this, while only using structural optimization to minimize deformations. Around a decade after the work of Chattopadhyay *et al.*, Sandak and Rosen [15] attempted to improve the performance of a rigid propeller blade with a flexible element in the root section. A multi-objective optimization procedure was applied to maximize the weighted efficiency in flight regimes characterizing climb and cruise, yielding an overall improvement in efficiency of between 7% and 17%, thus demonstrating the potential mission performance benefits of aeroelastic tailoring.

Sodja *et al.* [16] continued the work of Sandak and Rosen [15] through the development of an optimization procedure for the geometric design of a flexible propeller made from an isotropic material, with design variables corresponding to the blade axis geometry. The work of Sodja *et al.* consisted of aerodynamic optimization, allowable stress design, and blade-axis optimization. It was found that the deformation of the blade is heavily affected by the sweep angle, as the aerodynamic loads tended to deform the forward-swept (FB) blade opposite to the direction of rotation and away from the propeller plane, with the opposite effect occurring for the blade with zero or backward sweep [16]. The inertial forces always deformed the blade towards the

propeller plane. The result of this is that for propulsive operation, forward-swept blades exhibit an unfavourable wash-in effect that decreases the range of advance ratio values corresponding to high efficiency [16]. Backward-swept blades (BB) conversely have a favourable deformation with increasing freestream velocity and constant speed [16]. As the load increases, the bend-twist coupling results in a wash-out effect that increases off-design efficiency.

In addition to the journal publications that have been previously presented, multiple PhD theses have also been produced on the aeroelastic tailoring of propeller or wind turbine blades for yielding performance improvements. The earliest research was conducted by Khan [17], who developed a coupled propeller aerodynamic and structural analysis framework, and applied it towards the structural design of a flexible composite propeller. The ply orientations were adjusted to yield increases in the thrust coefficient, C_T, or efficiency, η_P, and decreases in the power coefficient, C_P. The same methodology was used to characterize the effect of bend-twist coupling on propeller performance in a subsequent paper published by Khan *et al.* [18]. In both works, it was shown that it is possible to yield noticeable increases or decreases in the thrust coefficient, power coefficient, and efficiency over a broad range of operating conditions through modifications of only the ply orientations of a flexible composite propeller with constant geometry. Moreover, Khan [17] was notably successful in improving on-design efficiency while maintaining the baseline thrust coefficient. Four notable PhD theses were produced at the TU Delft on aeroelastic tailoring of flexible wind turbine blades or aircraft wings using a similar gradient-based approach with lamination parameters as design variables in [19–22]. Optimization studies were completed for stall-regulated wind turbine blades by Ferede and Ferede *et al.* [19, 23], and for pitch-regulated wind-turbine blades by Hegberg and Hegberg *et al.* [20, 24]. Decreases in blade mass were observed through structural optimization in both works through the exploitation of extension-shear and bend-twist coupling to alleviate blade loads.

The research presented in this paper builds upon the preceding research of [13, 15–18, 25] by providing physical insights into how aeroelastic tailoring may benefit dual-role propeller performance, as previous work considered either only the structural design of propellers for the propulsive mode or the geometric design of flexible propellers. Thus, the goal of this work is to address suggestions made in [1, 2, 5] to design a propeller that provides a compromise between performance in propulsive and energy-harvesting modes through the implementation of the modern technique of aeroelastic tailoring, without including any changes in blade geometry. To satisfy this goal, the aeroelastic analysis method presented in [26] was integrated within an optimization procedure. Classical laminated plate theory has been used to represent the composite structure (like the work of [13, 17, 19, 20]) and a geometrically nonlinear beam model has been used to evaluate blade deformations (similar to the work of [16, 19, 20, 25]). Furthermore, structural properties of each laminate have been represented using lamination parameters, as was done in [19, 20], so all design variables remain continuous. Accordingly, the developed aeroelastic analysis routine was integrated within a gradient-based optimization framework. Through a mission-weighted objective function, the propulsive mode is accounted for through the minimization of energy consumption in climb and cruise, with energy-harvesting during the descent segment. As a result, both propulsive and energy-harvesting modes are included and weighted according to the time spent in each mission segment.

This paper is organized as follows: First, the developed aeroelastic optimization method is summarized in Section 2. An overview of the design study is provided next in Section 3. Following this, the results obtained from the design study are presented and discussed in Section 4. Finally, the main conclusions from this research are provided in Section 5.

2 PROPELLER ANALYSIS AND OPTIMIZATION OVERVIEW

2.1 Static Aeroelastic Analysis and Optimization Workflow

A complete overview of the aeroelastic model that was applied during this research is provided by Rotundo *et al.* [26]. For completeness, a brief description of this aeroelastic model is also provided in this section, as well as how it was integrated within the optimization framework.

The aeroelastic model that was applied during this research is a modified version of PROTEUS, which was previously developed and applied at the TU Delft towards the conceptual design of aircraft wings in [22, 27] and wind turbine blades in [19, 20]. Important characteristics of the model that was applied during this research are listed below. The structural model of PROTEUS is an application of the finite-element method to solve deformations on a reduced-order 1D Timoshenko beam element mesh. This 1D beam element mesh is obtained from the 3D blade structural geometry using the cross-sectional modeller from [28]. Blade deformations are caused by both the centrifugal and aerodynamic loads acting on the blade. Centrifugal loads are computed directly with the structural model, and the aerodynamic loads are computed using a blade element momentum (BEM) model. A BEM model was used because it has the lowest computational cost and is capable of accounting for viscous effects through the direct usage of airfoil polar data. The effect of rotation on the onset of flow separation has been accounted for through the use of RFOIL, which was developed using the stall-delay model proposed by Bosschers *et al.* [29]. This method was selected because it is based on a modification to the boundary layer equations, and does not rely on any empirical data. To combine the structural and aerodynamic models together within the aeroelastic model, a two-way coupled solver was developed and applied to ensure that structural deformations influence aerodynamic loads and vice versa. For this, a tightly coupled approach was developed and applied due to its robustness and fast convergence. The tightly coupled aeroelastic analysis proceeds using Newton's method iterations, with sensitivities that are computed analytically. The aeroelastic model was integrated within an optimization routine according to the schematic diagram shown in Fig. 2.1.

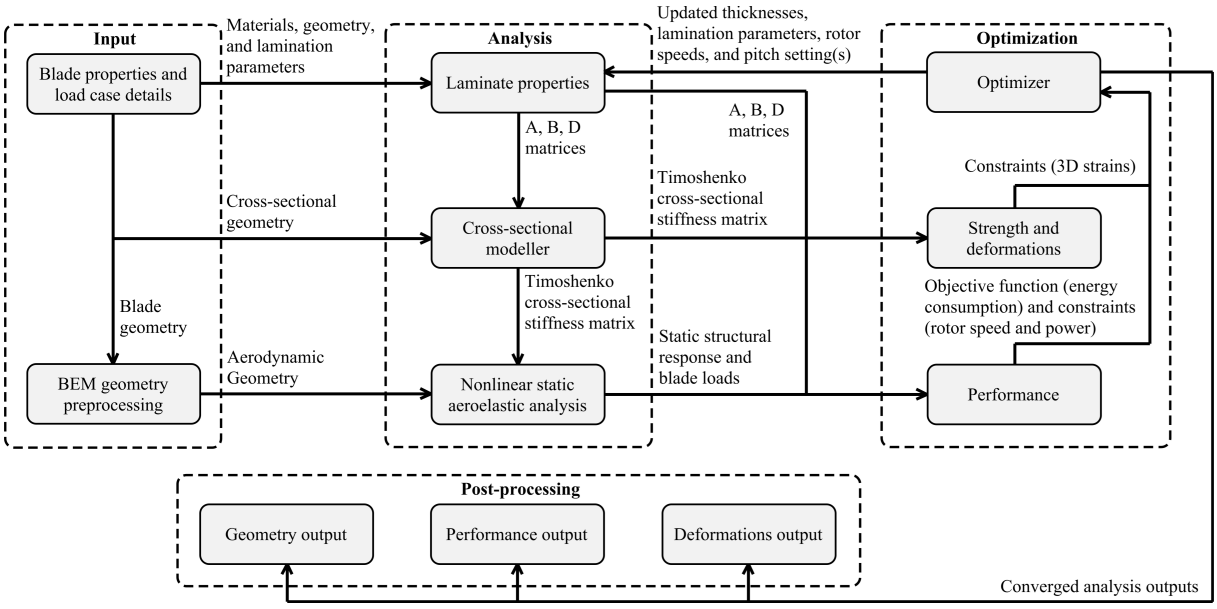

Fig. 2.1: A schematic representation of the static aeroelastic optimization routine.

As shown in Fig. 2.1, the optimization proceeds as follows: First, a pre-processing step is completed to define the geometry, operating conditions, and optimization inputs. After processing

all the inputs and collecting relevant parameters, the interpolated laminate properties and cross-sectional geometry are processed by the cross-sectional modeller to represent the structure as an equivalent finite element beam model. The optimization routine then proceeds by iteratively performing the aeroelastic analysis, to minimize the objective function that is defined in Section 2.2, while satisfying all constraints that are listed in Section 2.3. This minimization proceeds through a gradient-based approach, with sensitivities that are computed through a numerical central differencing scheme. A post-processing step is required to normalize the objective function, design variables, and constraints within each iteration of the optimization routine to ensure that the design variables are all scaled appropriately and also to increase the convergence rate. Descriptions of the design variables and normalization approach are respectively provided in Sections 2.4 and 2.5. A denormalization step is also completed before passing variables to the aeroelastic model because the aeroelastic analysis requires dimensional variables. Finally, the structural design, performance, and deformation outputs are recorded after convergence.

2.2 Objective Function

The optimization problem under consideration during this work is shown below in Eq. (2.1).

$$\begin{aligned} &\text{Minimize} && f\left(\underline{\Phi}\right) && \\ &\text{subject to} && g_i\left(\underline{\Phi}\right) \leq 0 && i \in \{1, \ldots, N_{\text{con, 1}}\} \\ &&& h_j\left(\underline{\Phi}\right) = 0 && j \in \{1, \ldots, N_{\text{con, 2}}\} \\ &\text{with bounds} && \Phi_k^{\text{L}} \leq \Phi_k \leq \Phi_k^{\text{U}} && k \in \{1, \ldots, N_{\text{var}}\} \end{aligned} \tag{2.1}$$

During optimization, the propeller performance was maximized over a fixed mission profile, with the objective function in this case being summed energy over the entire mission, computed using the corresponding shaft power and time spent in each mission segment, as indicated by Eq. (2.2). This metric was selected for the objective function because it ensures that both the propulsive and energy-harvesting modes are appropriately accounted for and weighted according to their relative contributions towards the overall mission energy consumption.

$$E\left(\underline{\Phi}\right) = \sum_{n=1}^{N_{\text{obj}}} P_n\left(\underline{\Phi}\right) \cdot t_n \tag{2.2}$$

By using the proposed single-objective optimization problem, all mission segments are considered together instead of separately. In this way, the proposed optimization objective is to minimize the weighted sum of the power consumption from each of the three mission segments, with the weighting factors being the time spent in each corresponding segment. Thus, the importance of each mission segment is determined by the time spent. This physical meaning behind the weighting factors of the optimization objective function was used to motivate the parametric study, as the length of the cruise segment was varied to assess the effect of mission definition on the optimal propeller design. Lastly, use of the power consumption as the optimization objective must be accompanied by equality constraints on the thrust in each segment to ensure that the propeller remains capable of satisfying all mission requirements. By maintaining a constant thrust requirement in each segment, any decrease in power consumption or increase in power generation will directly result in an improvement in efficiency.

2.3 Constraints

Both inequality and equality constraints were defined during the optimization. The only equality constraints considered during the optimization are for the thrust output in each mission segment.

By maintaining a constant thrust, it is ensured that any decreases in power consumption will not come at the cost of a decrease in thrust, and thus it is ensured that the optimized propeller can still meet the requirements of the mission. Because a three-segment mission profile was defined, there are three equality constraints in total. Inequality constraints, listed in Table 2.1, have been applied to ensure that the blade design and operating conditions remain feasible. First, inequality constraints defining known feasible regions for lamination parameters have been included to ensure that it is possible to extract a feasible ply stacking sequence from the resulting set of lamination parameters. Details on these feasible regions are reviewed by Albazzan *et al.* [30]. Due to the usage of lamination parameters for the parametrisation of the laminates, the strength constraint was implemented using the conservative allowable strain envelope based on the *Tsai-Wu failure criterion* [31, 32]. Lastly, the power consumption of the propeller was constrained in each mission segment by the maximum available shaft power, and tip displacements were constrained to prevent excessive deformations.

Table 2.1: A list of inequality constraints used during the optimization procedure.

Category	Constraint Name
Structural*	• Maximum normal strain (tensile), $\varepsilon^{\mathrm{T}}_{\mathrm{max}}$ • Minimum normal strain (compressive), $\varepsilon^{\mathrm{C}}_{\mathrm{min}}$ • Maximum shear strain, γ_{max} • Maximum tip displacement, p_{max}
Feasibility	• Feasible regions for lamination parameters
Performance	• Maximum shaft power, P_{max}

* See Appendix A for details on the maximum allowable stresses, which were used to compute maximum strains.

2.4 Design Variables

To proceed with the optimization, it is necessary to define design variables for the propeller's structural design as well as its operating conditions.

The blade structure consists of four structural elements, which are each defined by a single laminate of constant thickness. These four structural elements include a top and bottom skin as well as two spar webs. The spar webs have been assumed to be quasi-isotropic, and therefore their thicknesses are the only design variable required to ensure that they are completely defined. The upper and lower skins were assumed to feature symmetric laminates because asymmetric laminates are difficult to manufacture. To fully define the upper and lower skin structures, the stiffness properties are described by a set of eight lamination parameters that govern the membrane and bending stiffness, defined respectively by $\boldsymbol{A}$ and $\boldsymbol{D}$ matrices. Because all laminates are defined as symmetric, the coupling matrix, $\boldsymbol{B}$, is assumed to be equal to $\boldsymbol{0}$. In total, this yields 20 structural design variables to completely represent the blade structure. It is important to note that each surface was parametrized by a single laminate, although it is possible to consider multiple chordwise or spanwise laminates. This decision was made to maintain a low computational cost, although it may be possible to yield further enhancements in performance through the use of multiple spanwise or chordwise laminates in future work.

The remaining design variables define the propeller operating conditions, and they are the advance ratio and pitch setting values for each mission segment. During the optimization, both constant-pitch and variable-pitch propellers were evaluated, and thus either a single pitch setting is used for across the entire mission or a unique pitch setting is used for each mission segment.

2.5 Normalization

To ensure that the optimizer can correctly assess the sensitivities of the design variables, it is essential that the design vector, objective function, and constraints are normalized so that all variable values and function outputs are within approximately the same orders of magnitude.

The objective function is the total mission energy, which is normalized by the value corresponding to the rigid propeller, as shown in Eq. (2.3). This normalization was selected because the optimal rigid propeller performance is considered as the baseline during this work.

$$f\left(\underline{\Phi}\right) = \frac{E\left(\underline{\Phi}\right)}{\left|E_{\text{rigid}}\right|} \tag{2.3}$$

Each constraint function is normalized by their limit values, as shown in Eq. (2.4), where $k\left(\underline{\Phi}\right)$ is the evaluated inequality constraint value and k_{limit} is the limit value of the inequality constraint. This applies for all structural- and performance-related constraints from Table 2.1.

$$g_i\left(\underline{\Phi}\right) = \frac{k^i\left(\underline{\Phi}\right) - k^i_{\text{limit}}}{k^i_{\text{limit}}} \leq 0 \qquad\qquad i \in \left\{1\,, \ldots, N_{\text{con, 1}}\right\} \tag{2.4}$$

The same normalization was applied towards thrust equality constraints, as shown in Eq. (2.5)

$$h_j\left(\underline{\Phi}\right) = \frac{T^j\left(\underline{\Phi}\right) - T^j_{\text{required}}}{T^j_{\text{required}}} = 0 \qquad\qquad j \in \left\{1\,, \ldots, N_{\text{obj}}\right\} \tag{2.5}$$

Lastly, all design variables have been normalized to take values between -1 and 1 using Eq. (2.7), which requires the mean value between the bounds of each design variable. The mean value corresponding to each design variable is computed using Eq. (2.6).

$$\underline{\Phi}_0 = \frac{1}{2}\left(\underline{\Phi}^{\text{L}} + \underline{\Phi}^{\text{U}}\right) \tag{2.6}$$

As shown in Eq. (2.7), the normalization of the design vector is computed by subtracting the midpoint between the upper and lower bounds of the design vector from the original design vector and then multiplying this value by a so-called normalization matrix $\boldsymbol{N}$.

$$\hat{\underline{\Phi}} = \boldsymbol{N}\left(\underline{\Phi} - \underline{\Phi}_0\right); \qquad \boldsymbol{N} = \text{diag}\left\{\left(\frac{1}{2}\left(\underline{\Phi}^{\text{U}} - \underline{\Phi}^{\text{L}}\right)\right)^{-1}\right\} \tag{2.7}$$

3 DESIGN STUDY OVERVIEW

The operating conditions and thrust requirements that were held constant during the optimization studies are provided in Section 3.1. A discussion of the propeller blade design that was assumed during the optimization studies is subsequently provided in Section 3.2, followed by an overview of the optimization cases that were considered in Section 3.3.

3.1 Propeller Operating Conditions

Propeller operating conditions were defined after first establishing the mission strategy. During the propeller optimization study, only one mission profile was defined using performance characteristics that represent a typical general aviation aircraft within the *light sport* category. A notional diagram depicting the mission profile that was assumed during the design studies

is provided in Fig. 3.1. In each mission segment, operating conditions and thrust requirements were defined by a single operating point at the mean altitude of the segment. While it would be more precise to model the climb and descent phases with multiple operating points due to the changing altitude and operating conditions over the duration of these phases of the mission, the three-segment mission shown in Fig. 3.1 was used to maintain a low computational cost. Moreover, this three-segment mission remains sufficient for defining opposing operating conditions with appropriate weighting factors, as is the primary reason for its use during the design study.

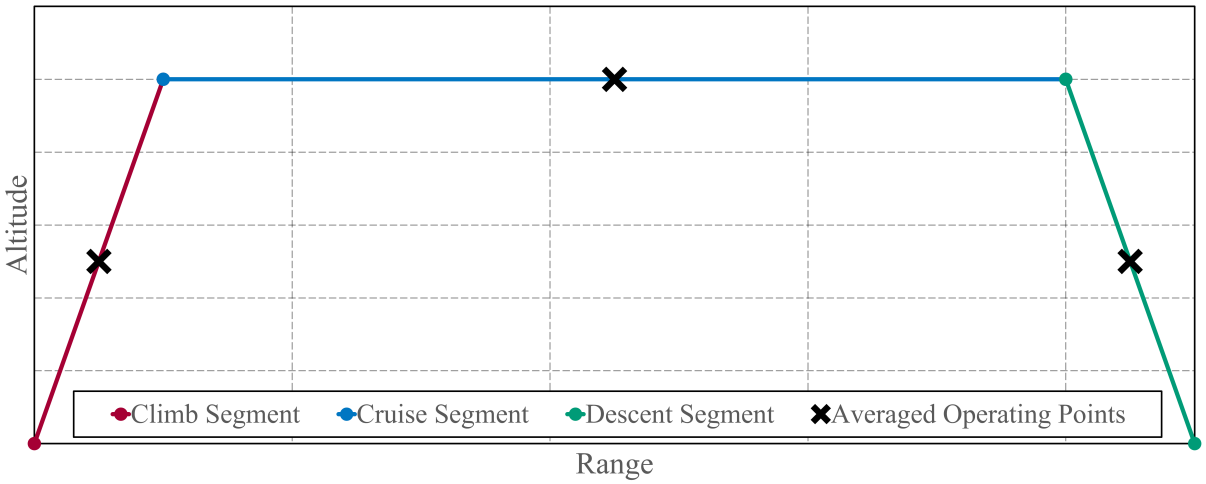

Fig. 3.1: A notional diagram of the mission profile that was evaluated during this research.

The averaged propeller operating conditions for each mission segment are provided in Table 3.1. A complete mission analysis including a reference aircraft was considered outside the scope of this research, although the values selected remain realistic for a typical *light sport* aircraft. The mission profile is only necessary to capture the differing requirements between the three mission segments, and the exact numbers that are selected are not expected to largely influence the general design trends yielded by the optimization studies.

Table 3.1: Quantities defining the climb-cruise-descent mission profile, derived from [33, 34].

Operating Condition	**Climb**	**Cruise**	**Descent**
Altitude (m)	1000	2000	1000
Flight Speed (m/s)	55	80	45
Climb Rate (m/s)	5.5	0.0	0.0
Descent Rate (m/s)	0.0	0.0	4.8
Distance covered (km)	20	{0, 50, 100, 150, 200, 400}	22
Approximate Time spent (min.)	6	{0, 10, 21, 31, 42, 83}	7
Thrust requirement (N)	2585	1780	-380
Maximum shaft power (kW)	200	200	200
T_C requirement	0.230	0.083	-0.051
Maximum P_C	0.323	0.116	0.590

In future work, it would be interesting to consider different mission profiles, to potentially identify biases and trends that arise during optimization studies due to the definition of the mission strategy. Indeed, it was noted in Section 1 that Erzen *et al.* [7] observed large improvements in the performance of dual-role propellers due to the selection of a mission strategy that benefits

from their use. Some alternative mission profiles that could be investigated with the proposed optimization approach include traffic pattern circuits, which were studied by Erzen *et al.* [7], or loiter-dash mission profiles, which were analysed by Dorfling and Rokhsaz [35]. The climb-cruise-descent mission was selected for this work because it is commonly performed by general aviation aircraft and conveniently includes both the propulsive and energy-harvesting modes, and it provides a realistic way of prioritizing each segment of the overall mission. Moreover, optimization studies were completed for varying cruise lengths to show how the blade design changes as the relative contribution of the energy-harvesting phase decreases.

3.2 Propeller Materials and Geometric Properties

The propeller blade geometry that was assumed in all optimization studies was obtained by scaling the TUD-XPROP-3, which was previously studied in [26]. The blade dimensions were scaled up by a factor of 4.5 (yielding a blade tip radius of 914.4 mm) to yield a blade of representative scale for application on a general aviation aircraft. This decision was made because including blade flexibility prevents results obtained on a scaled-down model from being scaled up to realistic flight conditions as the deformations between the scaled and full models will be of a different magnitude, unless the laminate stiffness properties are also adjusted. Geometry information for the TUD-XPROP-3 and composite laminate material properties are provided in Section 3.2 for completeness. Lastly, variable-pitch and constant-pitch versions of this propeller were considered to explore potential differences yielded in each configuration. In particular, both configurations must use one structural design to complete the mission, trading-off performance between mission segments, although the variable-pitch propeller maintains the ability to select different operating conditions in all mission segments and the constant-pitch propeller is restricted to one pitch setting for the whole mission. By evaluating both propeller types, it is possible to study how restricting the propeller operating conditions affects structural design trends. The optimal performance of the rigid variable-pitch propeller also provides an interesting baseline for both the optimal flexible constant- and variable-pitch propellers.

The propeller blade geometry is depicted in Fig. 3.2. As shown in this figure, two spar webs were placed at locations of $0.02c$ and $0.90c$ because the cross-sectional modeller used during the aeroelastic analysis could not represent the stiffness properties of the leading and trailing edge sections. By placing the font and rear spars as near as possible to the leading and trailing edges of the blade, the upper and lower surface skins remain the primary load-carrying components of the structure, and thus the spar webs have a small effect on the aeroelastic response.

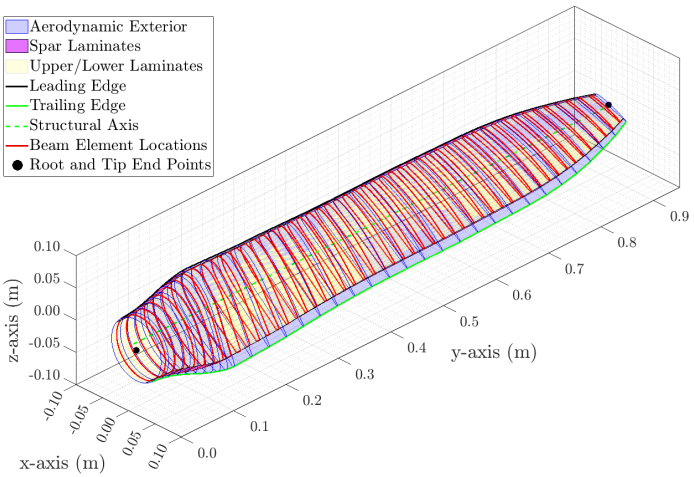

Fig. 3.2: A visual depiction of the blade geometry that was used during optimization studies.

Finally, the composite material chosen for all laminates is *AS4/APC2*. This material was selected for its high strength and moderate values for E_{11} and E_{22} in comparison to other carbon fibres. It also exhibits a large difference in stiffness between the two in-plane axes, as required for realizing the effects of aeroelastic tailoring. Information on the propeller geometry and material properties considered during this research are provided in Appendix A.

3.3 Overview of Optimization Cases

Motivated by the discussion from Section 1, to comprehensively assess the effect of the overall mission profile as well as the effect of individual mission segments on the optimum propeller design, three different design studies were completed. First, analyses were completed with the rigid propeller blade to obtain the rotor speed and pitch setting combinations yielding its ideal performance at all operating points under consideration during the optimization studies. These results enable the rigid propeller performance at its ideal pitch setting to be used as a baseline during the flexible propeller optimization studies, thus ensuring that all improvements in performance yielded by the flexible propeller in comparison to the rigid propeller are a direct result of applying aeroelastic tailoring. This step was also essential because the minimum energy consumption of the rigid propeller was used to normalize the objective function. After completing the rigid propeller analysis cases, flexible propeller optimization studies were performed for each mission segment individually to identify optimal blade structures and performance characteristics corresponding to each individual mission segment. These results were used to determine how closely the optimal blade designs obtained from the full-mission optimization studies align with results from each segment, to gain insight into the prioritization of each mission segment during full-mission optimization studies. These studies also provided the optimal flexible propeller performance in each individual segment, which was used as a theoretical upper-limit during the interpretation of results for the performance in each mission segment that was yielded by the propellers optimized over the entire mission. Finally, the full-mission optimization studies were completed for both constant-pitch (CP) and variable-pitch (VP) propellers over multiple cruise distances to complete the design study. Table 3.2 contains a list of cases that were investigated during optimization. To avoid converging on a local minimum, optimization studies were performed from several initial points and the converged feasible result yielding the smallest objective function was selected in each case.

Table 3.2: An overview of the flexible propeller optimization cases considered during this research.

#	Objective Type	Cruise Lengths (km)	Propeller Type
1	Climb Only	N/A	N/A
2	Cruise Only	N/A	N/A
3	Descent Only	N/A	N/A
4	Full Mission	0, 50, 100, 150, 200, 400	CP, VP

4 DESIGN STUDY RESULTS

Results for the ideal pitch settings, maximum efficiency, and minimum energy consumption of the rigid baseline propeller are shown in Section 4.1. After establishing a baseline, results obtained from the flexible propeller optimization studies are subsequently shown in Section 4.2.

4.1 Rigid Propeller Performance Trends

Fig. 4.1 contains results obtained from analyses of the baseline rigid propeller. Ideal pitch setting results are shown in Fig. 4.1a and 4.1c to respectively motivate the pitch settings used for

the baseline rigid propeller during flexible optimization studies of the variable- and constant-pitch propellers. The remaining two plots, Fig. 4.1c and 4.1d, contain results for the minimum energy consumption of the constant- and variable-pitch propellers over the full mission discussed in Section 3. The intention behind presenting these plots is to provide an idea of the difference in energy consumption between the constant- and variable-pitch propellers.

The baseline propeller performance considered during the flexible propeller optimization studies has been defined as the performance of the rigid propeller at its best pitch setting for each mission segment. For variable pitch propellers, this best pitch setting was found through an evaluation of the efficiency as a function of the pitch setting in each mission segment for a constant T_C, as plotted in Fig. 4.1a. The annotations shown in Fig. 4.1a correspond to the pitch settings that yielded peak efficiency. Energy consumption values yielded from the use of these blade pitch settings over the full mission with the variable-pitch propeller have been plotted in Fig. 4.1c and 4.1d. To identify the minimum total energy consumption of the rigid constant-pitch propeller, the total energy consumption over the full mission was evaluated at each pitch setting, for a range of cruise distances. At each cruise distance considered during this study, the pitch setting that was found to minimize the overall energy consumption was plotted in Fig. 4.1b, with its corresponding energy consumption plotted in Fig. 4.1c and 4.1d. Horizontal lines shown in Fig. 4.1b indicate the ideal pitch settings in each isolated segment.

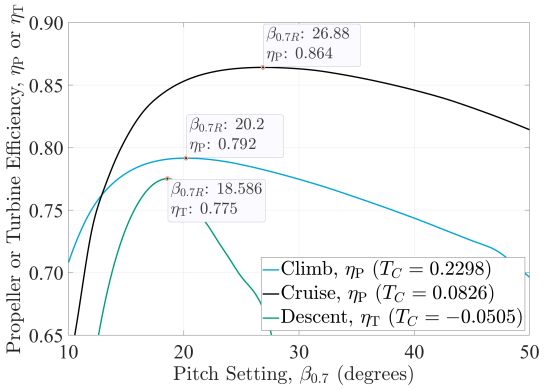

(a) Efficiency vs. pitch setting for each isolated mission segment considered during the design study.

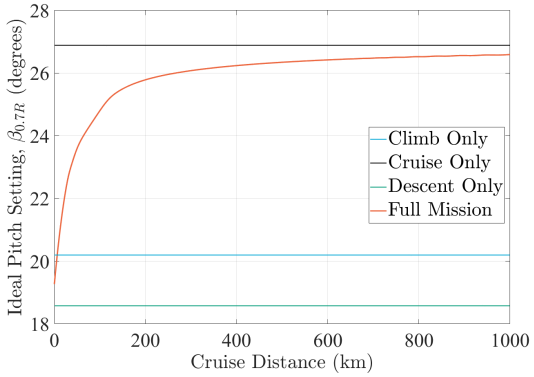

(b) Best pitch setting for the rigid constant-pitch propeller, plotted against the cruise distance.

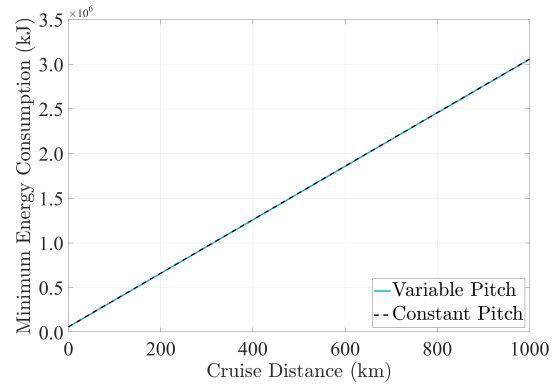

(c) Minimum energy consumption vs. cruise distance for the variable- and constant-pitch propellers.

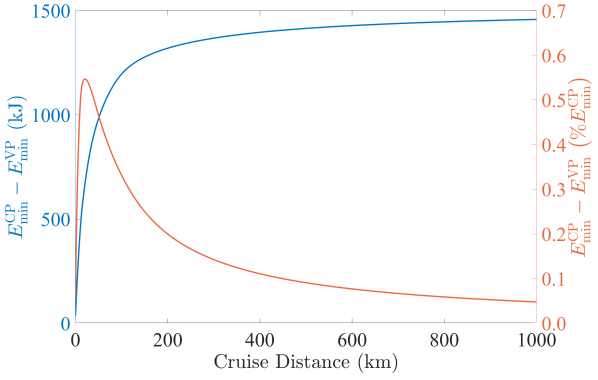

(d) Differences in minimum energy consumption between variable- and constant-pitch propellers.

Fig. 4.1: Performance trends for the rigid variable- and constant-pitch propellers under consideration.

The results shown in Fig. 4.1a and 4.1b for the ideal pitch settings of the rigid propeller remain consistent with general expectations. First, the optimal pitch setting is higher in the cruise

segment than in the climb segment due to the lower thrust requirement. During the descent, which has a negative thrust requirement, better performance is yielded at low pitch settings. The efficiency of the propeller in descent sharply decreases after its peak, as the maximum amount of negative thrust that the propeller can provide decreases rapidly with pitch setting. As shown in Fig. 4.1b, the best pitch setting of the constant-pitch propeller approaches the ideal pitch setting of the isolated cruise segment as the cruise distance increases. Because the climb and descent mission segments are of approximately equal weighting, when the cruise distance is zero, the best pitch setting is between the best climb and descent pitch settings. This trend is also apparent in Fig. 4.1d, where the difference in the minimum energy consumption of the constant- and variable-pitch propellers decreases as the cruise distance increases because the climb and descent segments contribute to a decreasing proportion of the total mission energy consumption. Nevertheless, the energy consumption values obtained for the rigid constant- and variable-pitch propellers remain within 1% of each other because the ideal pitch settings associated with the three mission segments are close to each other. This is also a result of the efficiency in climb and cruise changing by a small amount within the range of pitch settings corresponding to the constant-pitch propeller as the cruise distance increases, as shown in Fig. 4.1a. The climb and cruise efficiencies vary by less than 2% of their peak values over the range of pitch settings that yield ideal performance for the rigid constant-pitch propeller. In the descent segment, the efficiency decreases from its peak value by more than 10%, although the change in total energy consumption that is associated with this decrease in efficiency is small.

Despite the small difference in energy consumption between the constant- and variable-pitch propellers, both propeller types were considered during the flexible propeller design studies to provide initial insights into how the use of aeroelastic tailoring affects the performance and design trends in both configurations. It may be interesting to perform this same design study for a propeller that yields a larger difference in performance between its variable- and constant-pitch modes. For example, using the six-bladed *TUD-XPROP* would likely yield a larger difference in ideal climb-, cruise-, and descent-only pitch settings. This would result in the propeller exhibiting a noticeably larger total mission energy consumption, when treated as having a constant-pitch setting, in comparison to when allowing the propeller to have a variable-pitch setting.

4.2 Flexible Propeller Optimization

This section contains results obtained from the flexible propeller optimization studies. First, plots of the blade tip deformations and stiffness rosettes from the optimal structural designs are respectively presented in Sections 4.2.1 and 4.2.2 to provide insights into the presence of aeroelastic effects and the type of coupling that is exploited by the optimizer in each case that was considered. Following this, the optimal propeller operating conditions have been presented in Section 4.2.3 to provide insights into the pitch setting and advance ratio values and that were obtained during all optimization studies. Lastly, the most important performance trends, including plots for the efficiency and energy consumption in each mission segment, have been presented and compared with results for the ideal rigid propeller in Section 4.2.4.

Insights into the aeroelastic response, optimal structural designs, and optimal flexible propeller operating conditions presented in Sections 4.2.1 to 4.2.3 are imperative for contextualizing the performance trend results that are presented in Section 4.2.4.

4.2.1 Deformation Trends

Plots of torsional deformations and signed displacements at the blade tip have been provided in Fig. 4.2 as a function of the cruise distance. These deformation plots indicate the aeroelastic

response of the optimal blade designs at on-design conditions. For the signed tip displacement plots, positive displacements correspond to operation in propulsive conditions, and negative displacements correspond to operation in energy-harvesting conditions. This presentation of the displacements has been selected because the loading that is present during propulsive mode causes the blade to deform in the positive x- and z-axes, corresponding to Fig. 3.2, and loading that is present in energy-harvesting mode results in deformations in the negative x- and z-axes. These deformation plots, in combination with the stiffness rosettes shown in Fig. 4.3 and 4.4 of Section 4.2.2, are useful for demonstrating the type of coupling that is present.

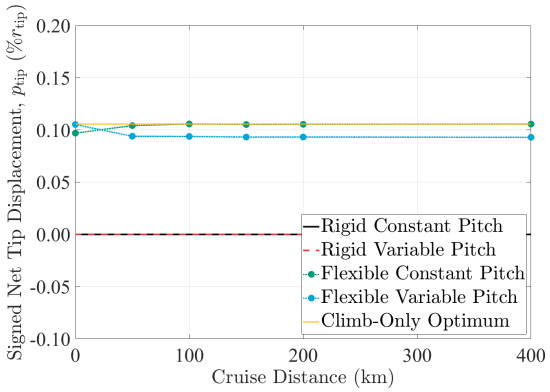

(a) Climb signed tip displacements

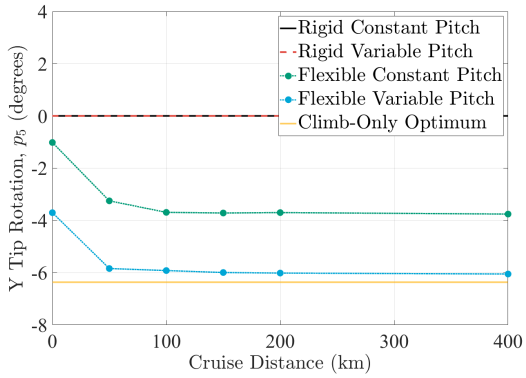

(b) Climb torsional deformations

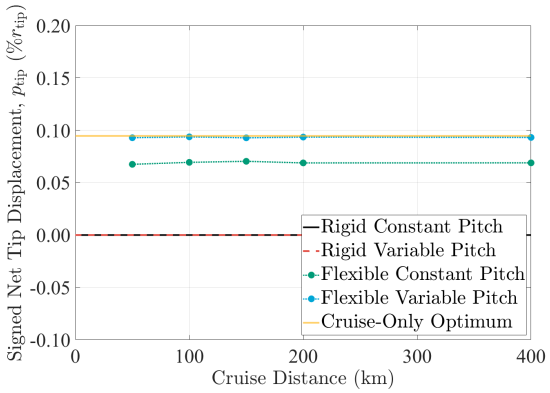

(c) Cruise signed tip displacements

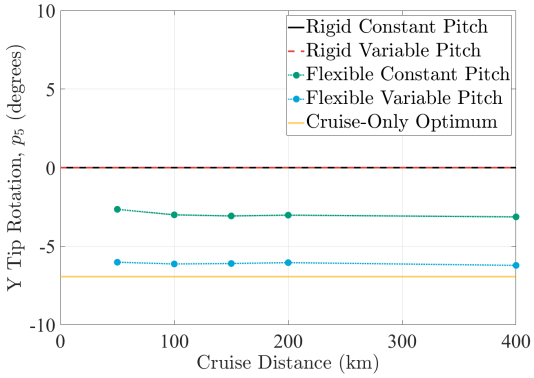

(d) Cruise torsional deformations

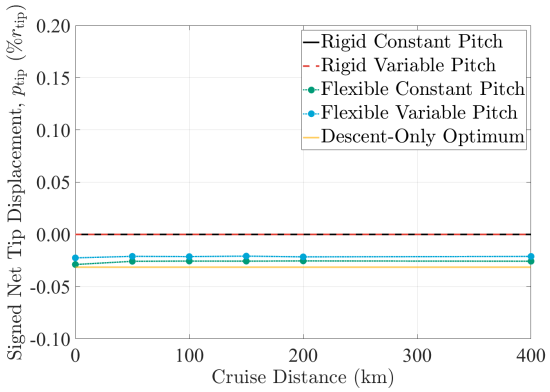

(e) Cruise signed tip displacements

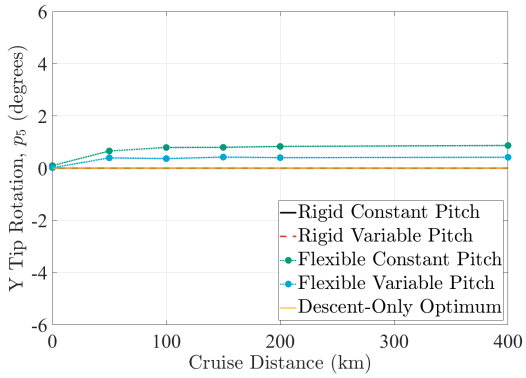

(f) Descent torsional deformations

Fig. 4.2: Deformation trends obtained for the optimal propeller configurations ($p_{tip} = \pm\sqrt{p_1^2 + p_2^2 + p_3^2}$).

First, plots of deformations in climb and cruise indicate similar trends, which is expected because the loading encountered by the propeller is similar in both cases. In particular, all propellers optimized for either the full mission or for the isolated climb or cruise segments appear

to exhibit an aerodynamic wash-out effect in propulsive mode, with positive tip displacements yielding negative torsional deformations. This result is consistent with the sensitivity studies that were presented by Rotundo *et al.* [26], where it was shown that introducing an aerodynamic wash-out effect can alleviate blade loads to result in a decrease in shaft power for a constant thrust setting. It is also clear from the plots of performance in propulsive mode (Fig. 4.2a to 4.2d) that the individual segment optimized blades yield the largest deformations and greatest amount of coupling, since their pitch deformations are consistently greater than that of the full-mission optimized blades. This is expected because the individual-segment optimized blades are only subjected to the objective and constraint functions for their corresponding mission segments, whereas the full-mission optimized blades must also balance requirements across the full mission, which result in a trade-off between the performance in each mission segment.

Concerning the full-mission optimized blades, the constant-pitch propellers appear to yield less of a wash-out effect in comparison to the variable pitch propellers, as indicated by the lower torsional deformations despite exhibiting greater tip displacements in climb when compared to the variable-pitch propeller. The flexible constant-pitch propeller has less of a wash-out effect than its variable-pitch counterpart because it is restricted to completing the full mission with only a single pitch setting, whereas the variable-pitch propeller can operate over a potentially broad range of pitch settings during the mission. As a consequence, the optimizer must restrict the twist deformations of the constant-pitch propeller through the use of less coupling, to balance opposing requirements in the different segments. Since the variable-pitch propeller can operate at multiple pitch settings, especially a high pitch setting in cruise and a low pitch setting in climb or descent, the optimizer can introduce a notably larger amount of wash-out to alleviate blade loads, while still guaranteeing ideal operating conditions for each individual segment.

Lastly, a different trend is interestingly observed during the descent segment. First, it is clear that the propeller blades optimized either for propulsive operation only or for the full mission continue to exhibit a wash-out effect in the descent, as expected, since negative displacements result in positive torsional deformations. However, the descent-optimized propeller does not appear to exhibit any pitch deformations as a result of its deflections. It is possible even for a slight wash-in effect to be present in this case, although it appears that the optimizer mainly decreased the twist deformations of the descent optimized blade. Furthermore, it is evident that the impact of blade flexibility is minimal during the energy-harvesting mode, as evidenced by the small tip displacements and torsional deformations depicted in Fig. 4.2e and 4.2f for all flexible blades that were analysed. This is expected, as the blade loading associated with energy-harvesting mode is minimal, due to the low freestream velocities and rotor speeds that characterize this regime. Accordingly, deformations exhibited in the descent are also small in contrast to the climb and cruise segments, thus reducing the effect of aeroelastic tailoring.

4.2.2 Optimal Structural Design Trends

Stiffness rosettes have been plotted to respectively indicate the in-plane and out-of-plane stiffness of each structural design obtained during optimization. Because only one laminate was used on the upper and lower surfaces of the blade, only a single stiffness rosette is required for each upper- and lower-surface laminate. The stiffness rosettes that were obtained during the optimization studies are shown in Fig. 4.3 for the upper surface and in Fig. 4.4 for the lower surface. Stiffness orientations are defined relative to the spanwise axis of the blade, positive toward the trailing edge on both upper and lower surfaces. Thus, a principal stiffness axis with an angle of 90° will point in the chordwise direction towards the leading edge, and a principal stiffness axis with an angle of 0° will point radially towards the blade tip.

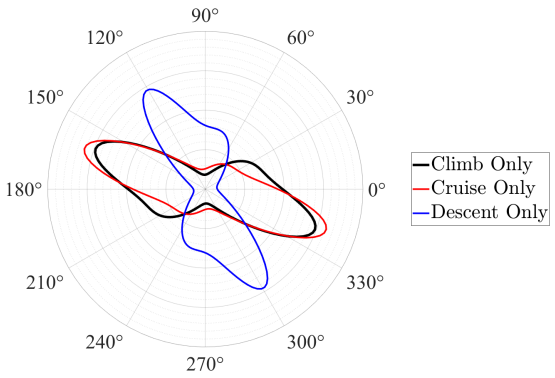

(a) In-plane (individual segments)

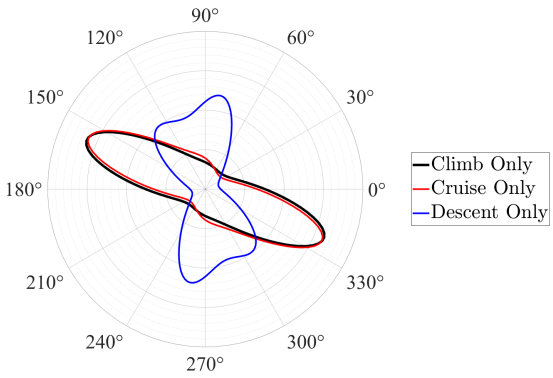

(b) Out-of-plane (individual segments)

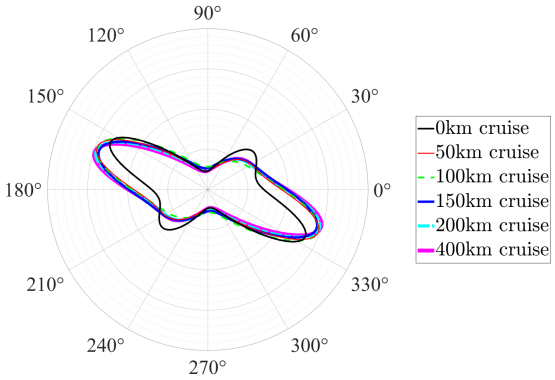

(c) In-plane (constant-pitch)

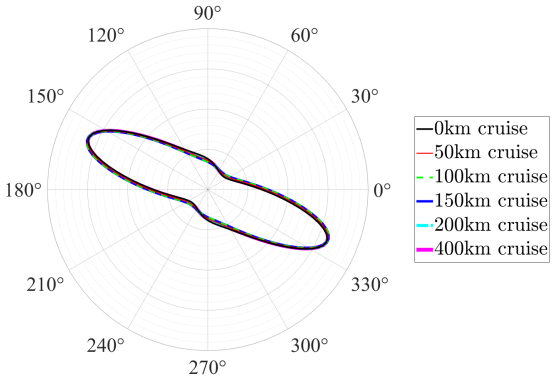

(d) Out-of-plane (constant-pitch)

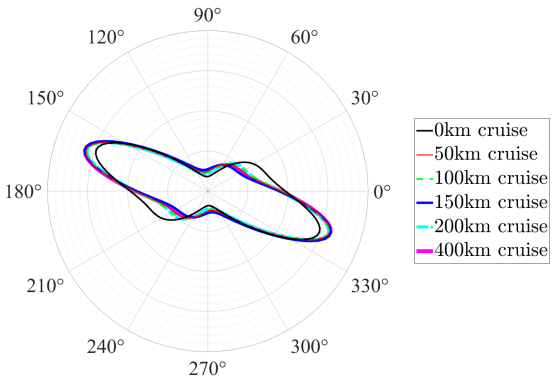

(e) In-plane (variable-pitch)

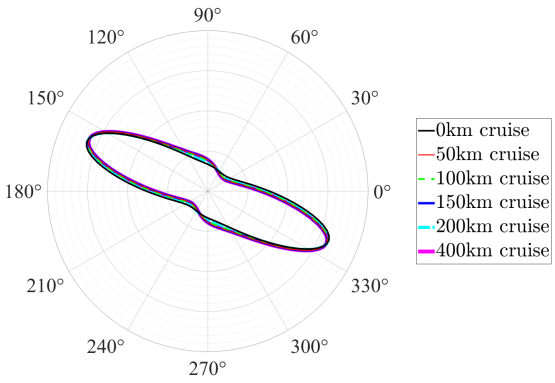

(f) Out-of-plane (variable-pitch)

Fig. 4.3: Upper surface stiffness rosettes obtained from optimization studies.

Starting with the individual mission optimization studies, the stiffness rosettes associated with the climb- and cruise-only optimization cases appear to have a similar shape on both the upper and lower surfaces, with the principle stiffness axis having an angle of approximately $-20°$ in either case. This is consistent with the sensitivity study results presented by Rotundo *et al.* [26], as it was found that ply orientations between $-30°$ and $-15°$ yielded the lowest power consumption at a constant thrust setting for all advance ratio values corresponding to the propulsive mode. The flexible propeller optimized for the isolated climb segment appears to deviate from this trend slightly, as the stiffness rosette of its lower surface laminate appears more balanced in comparison to the cruise-only rosette. This is because the loading is higher during climb in comparison to cruise, and thus the blade structure of the climb-only propeller must have more balanced stiffness properties to ensure that its strains remain within the allowable limit. When

considering only the propulsive mode, both the upper and lower surface rosettes exhibit the same general characteristic, and it is clear that the optimizer has converged on introducing a strong aerodynamic wash-out effect. Conversely, and consistent with deformation trends observed in Fig. 4.2, the optimal stiffness rosette configuration for the descent-only case appears considerably different from the ideal climb- and cruise-only results. In descent, it appears that the optimizer is introducing a wash-in effect on the upper surface and a wash-out effect on the lower surface, as the angle of the in-plane principal stiffness axis is near $+35°$ and the out-of-plane principal stiffness axis is near $+65°$ for the lower surface, and the angles of the in- and out-of-plane principal stiffness axes for the upper surface are respectively $-60°$ and $90°$. With angles further away from $90°$ on the lower surface, this blade may exhibit a slight wash-in effect, although it is difficult to discern any general trend from the results of this study alone.

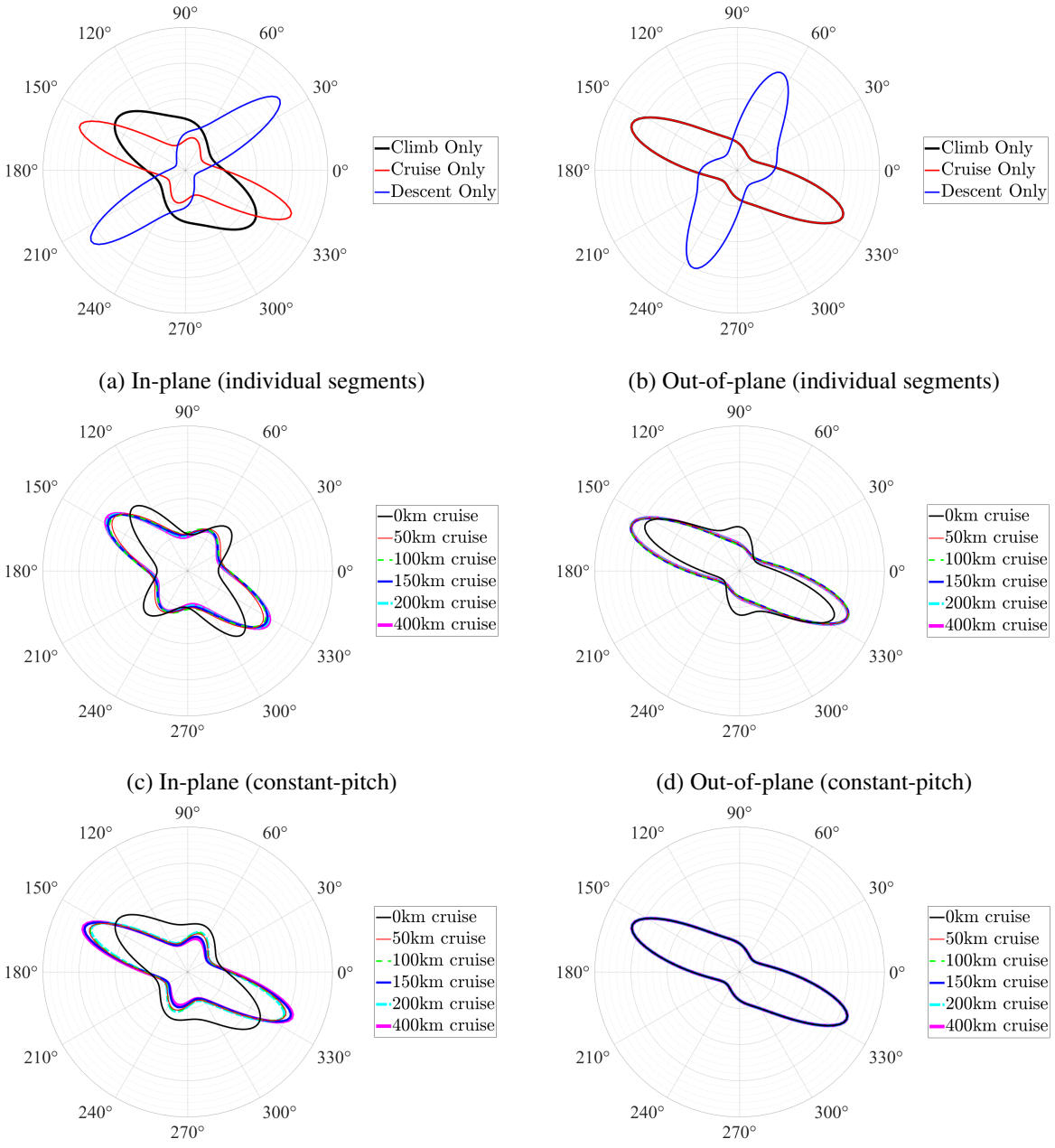

(a) In-plane (individual segments)

(b) Out-of-plane (individual segments)

(c) In-plane (constant-pitch)

(d) Out-of-plane (constant-pitch)

(e) In-plane (variable-pitch)

(f) Out-of-plane (variable-pitch)

Fig. 4.4: Lower surface stiffness rosettes obtained from optimization studies.

For both constant-pitch and variable-pitch propellers, the upper and lower surface laminates obtained by the optimizer yield the same stiffness rosette plots at all non-zero cruise distances under consideration. Additionally, similar stiffness rosettes appear to be obtained for both the constant- and variable-pitch cases, which appears to be a combination between the ideal stiffness distributions found during the climb- and cruise-only optimization cases. Moreover, like the isolated climb- and cruise-optimized propeller stiffness rosettes discussed previously, the stiffness distribution results for optimization studies involving the non-zero cruise distance appear consistent with the sensitivity studies that were performed by Rotundo *et al.* [26], with their principle stiffness axes also pointing at an angle of approximately $-20°$. When the cruise distance was set to zero kilometres, the upper and lower surface stiffness rosettes appear slightly different from the remaining stiffness rosettes, as the optimizer appears to be compensating slightly for the descent segment. Otherwise, the descent appears to be almost wholly neglected by the optimizer. The small amount of recovered energy in the descent, in addition to the reduced blade loading experienced during energy harvesting mode, is likely to be the reason for this. As a result, the flexible variable- and constant-pitch propellers are expected to exhibit a deteriorated energy-harvesting performance, as the ideal laminate configuration in climb or cruise is notably different from the ideal laminate configuration in descent. Therefore, in all full-mission optimization cases, a strong aerodynamic wash-out effect was introduced primarily to reduce power consumption in the climb and cruise segments, while incurring a decline in performance during the descent segment, consistent with trends shown in Fig. 4.2.

4.2.3 Propeller Operating Condition Trends

Propeller operating conditions observed from each optimization case are presented in Fig. 4.5. An important implication of this study is the strong influence that blade flexibility has on the optimal operating conditions of the propeller. In particular, results for the difference in pitch setting and advance ratio between the flexible and rigid propellers demonstrate that blade flexibility must be considered when searching for optimal propeller operating conditions. Moreover, the operating conditions associated with optimal flexible propeller performance may be difficult to predict in-flight, due to their dependency on blade loading. It is important to note that advance ratio trends follow from the pitch setting trends, where an increase in pitch setting results in an increase in advance ratio to maintain the same thrust setting.

Concerning results from the full-mission optimization studies, it is clear that the optimizer is prioritizing the climb and cruise segments heavily over the descent segment when considering both variable-pitch and constant-pitch propellers, consistent with trends shown in Sections 4.2.1 and 4.2.2. The low prioritization of the descent segment is attributed to the diminished impact of aeroelastic tailoring during the descent segment, as previously discussed, in addition to the limited proportion of the total mission energy that can be generated during energy-harvesting mode, particularly for longer cruise distances. Moreover, because of the low prioritization of the descent in comparison to the climb and cruise segments, the full-mission optimized propellers continue to exhibit an aerodynamic wash-out effect, which results in the optimal pitch setting of the flexible variable-pitch propeller being greater than that of its rigid version in the climb and cruise segments. Most notably, the pitch setting of the flexible constant-pitch propeller being very high and far from the optimal pitch setting of the flexible descent-only optimized propeller suggests that the optimizer neglected the descent segment for longer cruise distances. In particular, the optimal pitch setting curve of the flexible constant-pitch propeller appears to flatten beyond a cruise distance of 200 km at a value of $29°$, despite the flexible variable-pitch propeller reaching an even greater optimal pitch setting of $35°$. This occurs because the constant-pitch

propeller must maintain the negative thrust requirement in descent, and it is not possible for the required amount of negative thrust to be generated during the descent at pitch settings that exceed the maximum value that was reached by the flexible constant-pitch propeller.

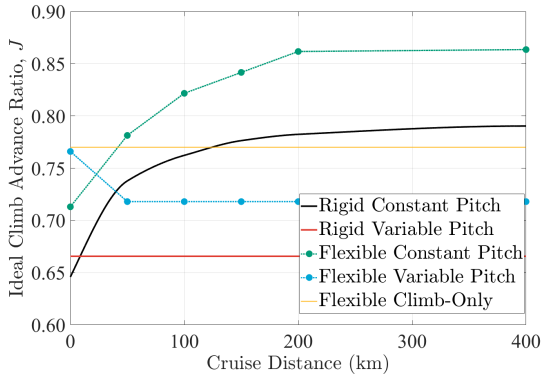

(a) Climb advance ratio

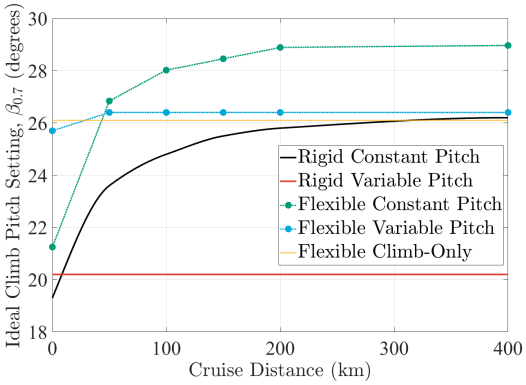

(b) Climb pitch setting

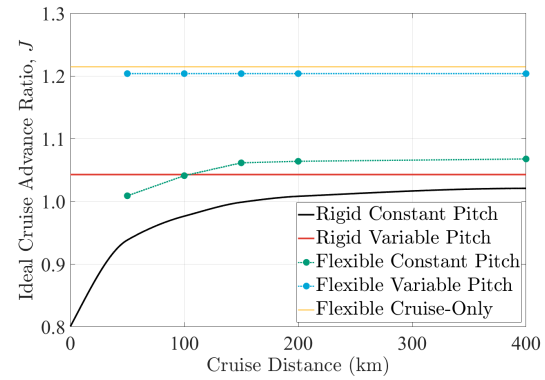

(c) Cruise advance ratio

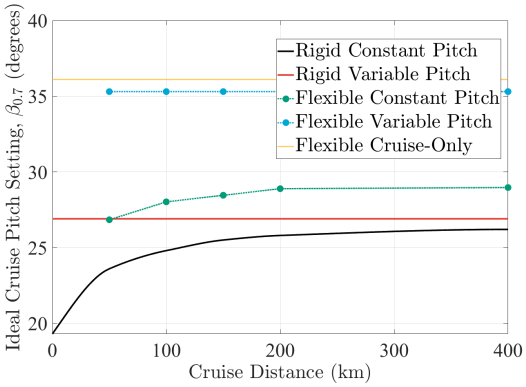

(d) Cruise pitch setting

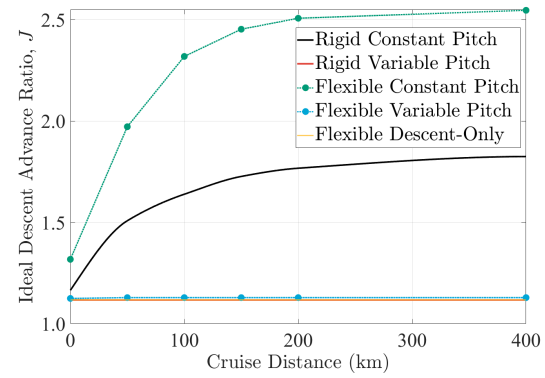

(e) Descent advance ratio

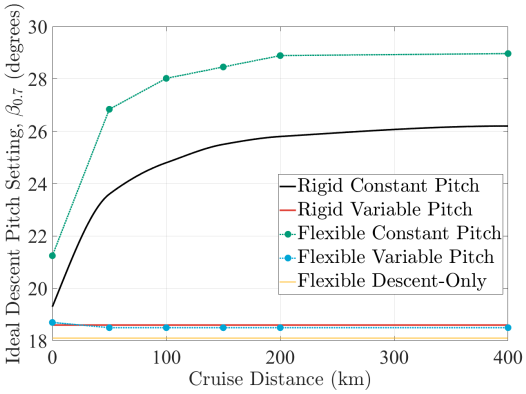

(f) Descent pitch setting

Fig. 4.5: Operating conditions for rigid and flexible optimal propeller configurations.

For the isolated climb- and cruise-only optimization cases, the ideal pitch setting of the flexible propeller tends to increase in comparison to that of the rigid propeller because the optimizer is exploiting the wash-out effect discussed in Sections 4.2.1 and 4.2.2 to enhance performance through the alleviation of blade loads. Resulting from this wash-out effect, when optimized either for isolated climb and cruise segments, or for the full mission, the pitch settings of the flexible propellers are shown to be noticeably greater than that of their rigid counterparts, as they exhibit pitch-down rotational deformations that cause the deformed blade shapes to have lower twist angles. For the isolated descent-only optimization case, the ideal pitch setting of the

flexible propeller is near to that of the rigid variable-pitch propeller because the low blade loading that characterizes energy-harvesting conditions makes aeroelastic tailoring less effective, as suggested by the descent-only propeller deformation trends from Fig. 4.2e and 4.2f.

4.2.4 Performance Trends

The optimal efficiencies for the rigid and flexible propellers are plotted in Fig. 4.6, the energy consumption results corresponding to these efficiency values are presented in Fig. 4.7.

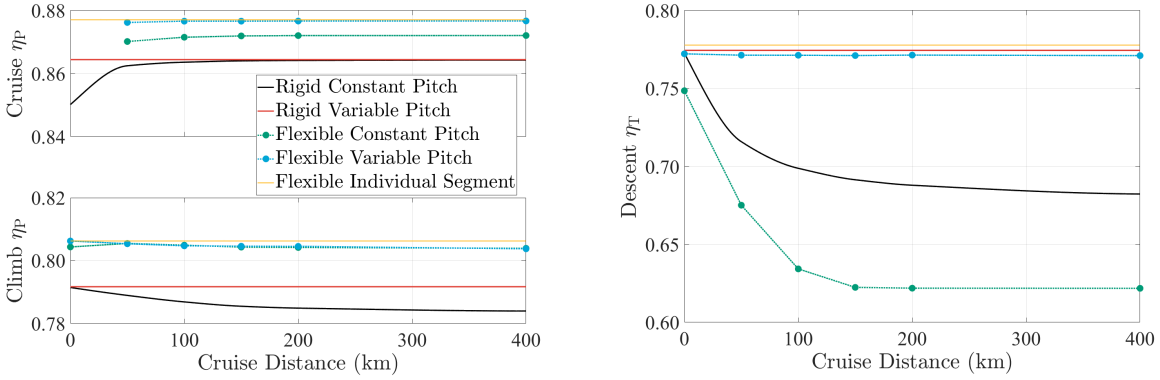

(a) Propeller efficiency (climb and cruise)

(b) Turbine efficiency (descent)

Fig. 4.6: Efficiencies corresponding to each optimal propeller configuration in each mission segment.

As expected, optimizing for each segment individually results in the greatest efficiency. It is interesting to observe that the full-mission optimization with a variable-pitch propeller yields efficiency values that are very close to the individual segment optimization results, independently of the cruise distance being considered. This is consistent with expectations in climb and cruise, where the ideal structural design between the two segments was shown to be similar in Fig. 4.3 and 4.4, and the full-mission optimization yielded similar structural designs to the ideal climb and cruise structures. However, in descent, it was shown that the ideal structural design differs considerably from the ideal structural design for the climb and cruise segments in Fig. 4.3 and 4.4. Despite this difference in structural design, the turbine efficiency of the ideal flexible variable-pitch propeller is very close to that of the rigid variable-pitch propeller and the isolated descent-optimized propeller. This occurs because the optimized flexible variable pitch propeller can still reach a pitch setting that is favourable for the descent segment, and it suggests that the effect of aeroelastic tailoring is small during energy-harvesting mode for variable-pitch propellers. The small influence of aeroelastic tailoring in the descent was also confirmed through the deformation plots presented in Fig. 4.2 of Section 4.2.1, highlighting that deformations associated with the descent segment are considerably smaller than deformations observed in the climb and cruise segments. This result is also aligned with the findings of Rotundo *et al.* [26], wherein it was demonstrated that variations in energy-harvesting performance due to blade flexibility are noticeably smaller than variations in propulsive performance.

For the optimal flexible constant-pitch propeller, the aforementioned small effect of aeroelastic tailoring during the descent is important. Because of the large influence of blade flexibility during the climb and cruise segments, outweighing the small influence of blade flexibility during the descent, the ideal pitch setting of the constant-pitch propeller is considerably higher than that of its rigid counterpart, as shown in Fig. 4.5. This is also a result of the fact that a small amount of energy is harvested during the descent in comparison to the total mission energy consumption. The reduced loading in the descent segment results in a small amount of addi-

tional positive twist deformations of the flexible constant-pitch propeller, as shown in Fig. 4.2f, thereby increasing the pitch setting to an even less optimal value. Nevertheless, because the blade loading in descent is small, it is still possible for the flexible constant-pitch propeller to complete the mission with a large pitch setting. Lastly, this large and uncompensated pitch setting of the flexible constant-pitch propeller notably reduces performance during descent, as it accordingly exhibits the lowest turbine efficiency in comparison to all other propeller types.

It is clear from Fig. 4.6 that the climb performance of the flexible constant-pitch propeller remains very similar to that of the flexible variable-pitch propeller, although a consistent gap emerges between the cruise efficiency of the flexible constant- and variable-pitch propellers, independent of cruise distance. This is because the optimizer must always maintain the thrust requirement in descent, due to the equality constraints that were imposed. Thus, it is likely that the pitch setting of the constant-pitch propeller cannot be increased beyond a value of approximately 29° while still maintaining the required negative thrust in descent. It is for this reason that the turbine efficiency of the flexible constant-pitch propeller reaches an excessively low value, before levelling off beyond a cruise distance of 150 km. If the negative thrust requirement in descent were reduced in magnitude or removed, then the efficiency of the constant-pitch propeller in cruise would approach the efficiency of the variable-pitch propeller as the cruise distance increased, and the climb efficiency of the constant-pitch propeller may accordingly decrease. Despite the optimal flexible constant-pitch propeller being forced to remain at a suboptimal pitch setting during the majority of the optimization cases, it remarkably maintains a lower total energy consumption than both the rigid constant- and variable-pitch propellers, as shown in Fig. 4.7. This clearly occurs as a result of the superior efficiency of the flexible constant-pitch propeller during the climb and cruise segments in comparison to both rigid propeller types.

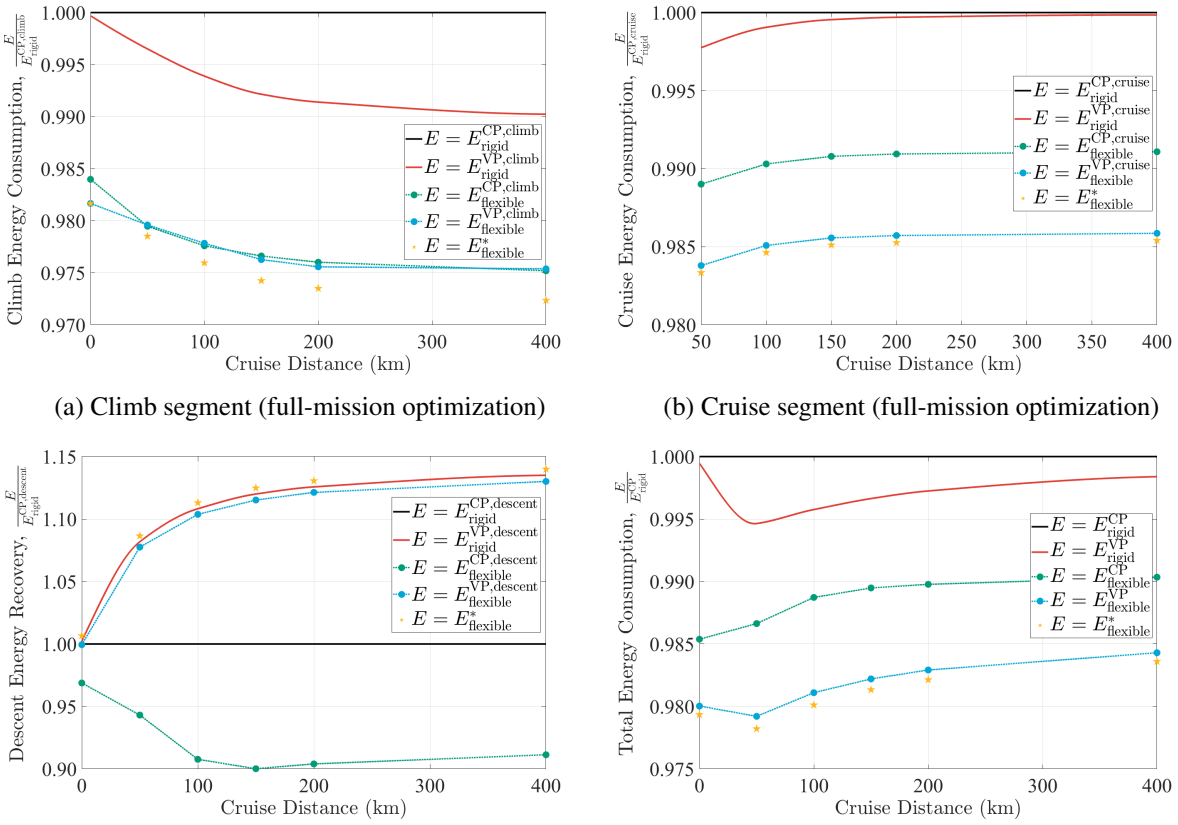

(a) Climb segment (full-mission optimization)

(b) Cruise segment (full-mission optimization)

(c) Descent segment (full-mission optimization)

(d) Total mission (objective function)

Fig. 4.7: Mission energy consumption or recovery compared between different optimal propellers.

In Fig. 4.7, E^* represents a theoretical maximum improvement that may be achieved through aeroelastic tailoring of propellers. This was computed using the energy consumption of the optimal flexible climb-only propeller in climb, the optimal flexible cruise-only propeller in cruise, and the optimal flexible descent-only propeller in descent. It is important to note that the energy consumption contributions from the climb, cruise, and descent segments used to compute E^* came from the individual segment-optimized flexible propellers, and therefore the propeller structural design and operating conditions are different in each mission segment. Hence, with one structural design alone, as is the case for the flexible constant- and variable-pitch propellers, it is likely not possible to obtain the same decrease in total mission energy consumption that is observed for E^* in Fig. 4.7d. It is thus useful instead to note values for E^* as theoretical upper-limits on the extent that performance may be enhanced through aeroelastic tailoring, given the fixed geometry that was considered and the fact that only one laminate was used for each surface of the blade. Lastly, it is interesting to observe that energy consumption or recovery values of the optimal flexible variable-pitch propeller are close to this upper limit.

Results for the energy consumption in each individual mission segment follow directly from the efficiency results shown in Fig. 4.6. The results for the total energy consumption, as depicted in Fig. 4.7d, are highly encouraging, as it appears that the flexible constant- and variable-pitch propellers consistently yield a lower total energy consumption than their rigid counterparts. Due to the somewhat high negative thrust requirement in descent, the flexible constant-pitch energy consumption never converges towards the flexible variable-pitch energy consumption, and instead appears to maintain an almost constant offset beyond cruise distances of 100 km. It is expected that if the constraint on thrust required during descent were relaxed, then the energy consumption of the flexible constant-pitch propeller would converge toward the energy consumption of the flexible variable-pitch propeller beyond a cruise distance of 50 km. Nevertheless, when compared with the rigid variable-pitch propeller across all optimization cases, the energy consumption decrease by $1.5 - 2.0\%$ for flexible variable-pitch propellers and by $0.7 - 1.4\%$ for flexible constant-pitch propellers is already quite substantial. In comparison to the rigid constant-pitch propeller, the decrease in energy consumption is even greater, at approximately $1.5 - 2.0\%$ for flexible variable-pitch propellers and $1.0 - 1.5\%$ for flexible constant-pitch propellers. Finally, the similar values yielded between the flexible variable-pitch and theoretical maximum performance improvement suggests that it may not be possible to yield any significant further decreases in total energy consumption unless more spanwise and chordwise laminates are used to represent each surface of the propeller blade structure.

5 CONCLUSIONS

An aeroelastic tailoring procedure was developed using the static aeroelastic analysis methodology that is documented in [26]. The developed optimization procedure was then applied towards the structural blade design of a composite variable-pitch or constant-pitch propeller for a typical *light sport* aircraft, based on a representative climb-cruise-descent mission profile with constant thrust requirements in each segment. The optimization objective was to reduce the total energy consumption, either over the full mission or over each segment individually. Constraints on laminate feasibility, as well as the maximum allowable shear and normal (tensile and compressive) strains, tip displacements, and shaft power were applied during the optimization to guarantee a converged design that is feasible both structurally and for the aircraft configuration of interest. The design variables considered during optimization consist only of the laminate thicknesses and lamination parameters, although it is possible to also include the geometric design of the propeller blade in future. After completing the optimization studies, deformations, structural

design trends, operating conditions, and performance characteristics corresponding to the flexible and rigid propellers were subsequently evaluated and compared. These results indicate the extent that performance may be improved solely through the use of aeroelastic tailoring.

After optimization, propellers that were optimized for the isolated climb and cruise segments featured similar structural designs with a strong aerodynamic wash-out effect, whereas the propeller that was optimized for the isolated descent segment featured a notably different structural design with minimal torsional deformations. In addition, both the constant- and variable pitch propellers that were optimized over the full mission featured a similar structural design to the propellers that were optimized for the isolated climb and cruise segments, with a noticeable aerodynamic wash-out effect. These findings suggest that the optimizer heavily prioritized the climb and cruise segments over the descent segment in all full-mission optimization cases.

After observing noticeable differences in ideal propeller operating conditions obtained for the optimal rigid and flexible propellers, it was found that blade flexibility has a strong influence on the pitch setting and advance ratio values that yield a minimum total energy consumption. The largest differences in operating conditions were observed in the climb and cruise segments due to the higher blade loading encountered in these segments, with all propellers except the flexible constant-pitch propeller maintaining similar operating conditions during the descent after optimization. The pitch setting of the optimal flexible constant-pitch propeller was also found to be restricted to ensure that it can satisfy the thrust requirement during the descent segment. Furthermore, because the optimizer tended to prioritize the climb and cruise segments, the flexible constant-pitch propeller was forced to operate at a high pitch setting that is suboptimal for the descent segment. Lastly, as a result of this trend in pitch setting, the flexible constant-pitch propeller experienced a notable decline in energy-harvesting performance after optimization.

All flexible propellers yielded better performance than their rigid counterparts after optimization. Despite the significantly degraded energy-harvesting performance of the flexible constant-pitch propeller, its energy consumption was consistently found to be below that of both the rigid constant- and variable-pitch propellers. For the flexible constant-pitch propeller, decreases in total energy consumption by $0.7 - 1.4\%$ and $1.0 - 1.5\%$ were respectively found in comparison to the rigid variable- and constant-pitch propellers after optimization. For the optimal flexible variable-pitch propeller, a decrease in energy consumption of $1.5 - 2.0\%$ was found in comparison to both the rigid constant-pitch and rigid variable-pitch propellers. In each individual mission segment, the flexible variable-pitch propeller exhibited comparable performance to that of the optimal blade designs obtained through the isolated mission segment optimization studies. This suggests that optimization of the flexible variable-pitch propeller has the potential to result in performance improvements that are close to the upper-limit of what may be obtained solely through aeroelastic tailoring. Further enhancements in propeller performance may be achieved by including modifications to the blade geometry during the optimization studies, in addition to using more spanwise and chordwise laminates to represent the blade structure.

ACKNOWLEDGEMENTS

Jatinder Goyal, cited as Goyal *et al.* [8], provided the BEM code that was used within the aerodynamic model of the optimization routine, in addition to polar plots from RFOIL for the TUD-XPROP, as required for all aerodynamic analyses performed during optimization. Noud Werter and Roland De Breuker, cited as Werter and De Breuker [36], largely developed the aeroelastic tailoring procedure called PROTEUS. PROTEUS was modified for this research to be applicable for propellers, although a substantial portion of the code remained unchanged.

A PROPELLER BLADE GEOMETRY AND MATERIAL PROPERTIES

This section respectively contains information on the propeller blade geometry and the materials used during this research. The information provided in this section was held constant throughout the full propeller design study that was conducted during this research.

TUD-XPROP-3 Geometry

Geometry data for the XPROP or XPROP-3 propeller are shown in Fig. A.1. The blade pitch setting is always defined as the twist angle at the 70% span position. Thus, the twist distribution that is shown in Fig. A.1b corresponds to a blade pitch setting of approximately $0°$.

Blade geometry information for the TUD-XPROP or TUD-XPROP-3 propeller is provided by Nederlof *et al.* [9]. There are two composite propellers with the same blade geometry and either three or six blades (XPROP-3 and XPROP, respectively). The incidence angle of the blades can be manually adjusted, and the diameter of the propeller is 406.4 millimetres. The propeller represents a typical previous-generation turboprop propeller, and thus its performance may be improved through geometry optimization for improved aerodynamic performance. It has negligible sweep and lean, making its geometry relatively simple, and the two discussed rotors that feature this blade geometry have been used extensively already for investigations into isolated propeller aerodynamics or aeroacoustics, propeller integration studies, and distributed propeller studies in [6, 8, 9]. The TUD-XPROP-3 was used exclusively during this research.

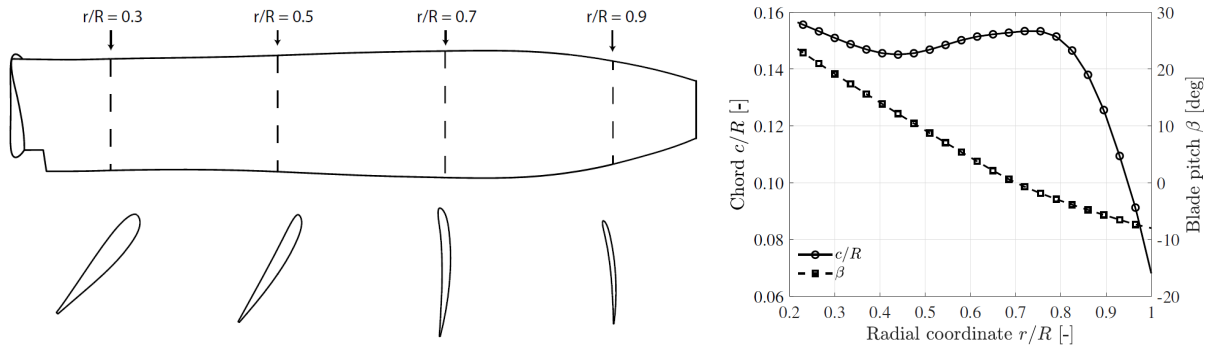

(a) Airfoils at varying spanwise locations. (b) Chord and twist distributions.

Fig. A.1: Geometric data for the TUD-XPROP propeller [9].

Material Data

Table A.1 contains a summary of the *AS4 / APC2* composite material that was used for the propeller under consideration during this research, referenced primarily in Section 3.2. Only unidirectional carbon fibres have been considered because they exhibit a good combination of strength and stiffness, therefore maximizing the effect of aeroelastic tailoring [37]. The subscript "11" denotes quantities acting parallel to the plies, while quantities acting orthogonal to the plies are denoted by the subscript "22". Ultimate tensile strength is denoted by the superscript "UT", the ultimate compressive strength is denoted by the superscript "UC".

Table A.1: Material properties used during the design problem under consideration [37, 38].

Material[a,b]	ρ_S	E_{11}	E_{22}	G_{12}	ν_{12}	σ_{11}^{UT}	σ_{11}^{UC}	σ_{22}^{UT}	σ_{22}^{UC}	τ_{12}^{U}
AS4 / APC2	1.57	134	8.70	5.1	0.28	2060	1100	78	196	157

[a] Fibre composite materials are conventionally named as follows: "fibre material" / "resin composition".

[b] SI units are used for all dimensional quantities listed in this table, with g/cm^3 for density values (ρ), GPa for elastic moduli (E, G), as well as MPa for ultimate compressive and tensile strength values (σ, τ).

REFERENCES

[1] Glauert, H., *The Analysis of Experimental Results in the Windmill Brake and Vortex Ring States of an Airscrew*, Her Majesty's Stationery Office, 1926.

[2] MacCready, P., "Regenerative Battery-Augmented Soaring," *Technical Soaring*, Vol. 23, No. 1, 2022, pp. 28–32.

[3] Barnes, J. P., "Math Modeling of Propeller Geometry and Aerodynamics," Tech. Rep. 1999-01-1581, The Society of Automotive Engineers (SAE), 1999. https://doi.org/10.4271/1999-01-1581.

[4] Barnes, J. P., "Flight Without Fuel – Regenerative Soaring Feasibility Study," Tech. Rep. 2006-01-2422, The Society of Automotive Engineers (SAE), 2006. https://doi.org/10.4271/2006-01-2422.

[5] Barnes, J. P., "Regenerative Electric Flight Synergy and Integration of Dual role Machines," *53rd AIAA Aerospace Sciences Meeting*, American Institute of Aeronautics and Astronautics, 2015, pp. 1 – 15. https://doi.org/10.2514/6.2015-1302.

[6] Sinnige, T., Stokkermans, T., van Arnhem, N., and Veldhuis, L. L., "Aerodynamic Performance of a Wingtip-Mounted Tractor Propeller Configuration in Windmilling and Energy-Harvesting Conditions," *AIAA Aviation 2019 Forum*, American Institute of Aeronautics and Astronautics, 2019, pp. 1 – 17. https://doi.org/10.2514/6.2019-3033.

[7] Erzen, D., Andrejasic, M., and Kosel, T., "An Optimal Propeller Design for In-Flight Power Recuperation on an Electric Aircraft," *2018 Aviation Technology, Integration, and Operations Conference*, American Institute of Aeronautics and Astronautics, 2018, pp. 1 – 9. URL https://arc.aiaa.org/doi/abs/10.2514/6.2018-3206.

[8] Goyal, J., Avallone, F., and Sinnige, T., "Isolated propeller aeroacoustics at positive and negative thrust," *Aerospace Science and Technology*, Vol. 147, 2024. https://doi.org/10.1016/j.ast.2024.109021.

[9] Nederlof, R., Ragni, D., and Sinnige, T., "Experimental Investigation of the Aerodynamic Performance of a Propeller at Positive and Negative Thrust and Power," *AIAA Aviation 2022 Forum*, American Institute of Aeronautics and Astronautics, 2022, pp. 1 – 22. https://doi.org/10.2514/6.2022-3893.

[10] Binder, N., Courty-Audren, S.-K., Duplaa, S., Dufour, G., and Carbonneau, X., "Theoretical Analysis of the Aerodynamics of Low-Speed Fans in Free and Load-Controlled Windmilling Operation," *Journal of Turbomachinery*, Vol. 137, No. 10, 2015. https://doi.org/10.1115/1.4030308.

[11] Munk, M. M., "Propeller Containing Diagonally Disposed Fibrous Material," Tech. Rep. 2484308, United States Patent Office, October 1949.

[12] Wood, T. H., and Ramakrishnan, K., "Aeroelastically Tailored Propellers for Noise Reduction and Improved Efficiency in a Turbomachine," Tech. Rep. 20150344127, US Patent Application, December 2015.

[13] Dwyer, W. J., and Rogers, J. B., "Aeroelastically Tailored Propellers," SAE Technical Paper 770455, SAE International, 1977. https://doi.org/10.4271/770455.

[14] Chattopadhyay, A., McCarthy, T. R., and Seeley, C. E., "Decomposition-based optimization procedure for high-speed prop-rotors using composite tailoring," *Journal of Aircraft*, Vol. 32, No. 5, 1995, pp. 1026–1033. https://doi.org/10.2514/3.46832.

[15] Sandak, Y., and Rosen, A., "Aeroelastically adaptive propeller using blades' root flexibility," *The Aeronautical Journal*, Vol. 108, 2004, pp. 411–418. https://doi.org/10.1017/S0001924000000221.

[16] Sodja, J., Drazumeric, R., Kosel, T., and Marzocca, P., "Design of Flexible Propellers with Optimized Load-Distribution Characteristics," *Journal of Aircraft*, Vol. 51, No. 1, 2014, pp. 117–128. https://doi.org/10.2514/1.C032131.

[17] Khan, A. M., "Flexible composite propeller design using constrained optimization techniques," Ph.D. thesis, Iowa State University, 1997. URL https://dr.lib.iastate.edu/handle/20.500.12876/64733.

[18] Khan, A. M., Dayal, V., Vogel, J. M., and Adams, D. O., "Effects of Bend–Twist Coupling on Composite Propeller Performance," *Mechanics of Composite Materials and Structures*, Vol. 7, No. 4, 2000, pp. 383–401. https://doi.org/10.1080/10759410050201717.

[19] Ferede, E. A., "Static Aeroelastic Optimization of Composite Wind Turbine Blades Using Variable Stiffness Laminates: Exploring Twist Coupled Composite Blades in Stall Control," Ph.D. thesis, Delft University of Technology, 2016. https://doi.org/10.4233/uuid:b4fe0ca4-b8c7-4e23-a2f1-247ac3b61aeb.

[20] Hegberg, T., "Fast Aeroelastic Analysis and Optimisation of Large Mixed Materials Wind Turbine Blades," Ph.D. thesis, Delft University of Technology, 2019. https://doi.org/10.4233/uuid:643ddf12-97d3-48a1-9742-b4dd22f16164.

[21] De Breuker, R., "Energy-based Aeroelastic Analysis and Optimisation of Morphing Wings," Ph.D. thesis, Delft University of Technology, 2011. URL http://resolver.tudelft.nl/uuid:867c84ae-6cf5-45aa-ba5f-ab6ec4bbf5ed.

[22] Werter, N. P. M., "Aeroelastic Modelling and Design of Aeroelastically Tailored and Morphing Wings," Ph.D. thesis, Delft University of Technology, 2017. https://doi.org/10.4233/uuid:74925f40-1efc-469f-88ee-e871c720047e.

[23] Ferede, E., Abdalla, M. M., and van Bussel, G. J. W., "Isogeometric based framework for aeroelastic wind turbine blade analysis," *Wind Energy*, Vol. 20, No. 2, 2017, pp. 193–210. https://doi.org/https://doi.org/10.1002/we.1999.

[24] Hegberg, T., de Breuker, R., and van Bussel, G. J. W., "Nonlinear Static Aeroelastic Design Case Studies of Large Offshore Wind Turbine Blades," *Proceedings of the EWEA conference 2013, Vienna, Austria*, EWEA, 2013, pp. 1–5.

[25] Sodja, J., De Breuker, R., Nozak, D., Drazumeric, R., and Marzocca, P., "Assessment of low-fidelity fluid–structure interaction model for flexible propeller blades," *Aerospace Science and Technology*, Vol. 78, 2018, pp. 71–88. https://doi.org/10.1016/j.ast.2018.03.044.

[26] Rotundo, C., Sinnige, T., and Sodja, J., "Aeroelastic Model for Design of Composite Propellers," *Proceedings of the AIAA SciTech 2024 Forum*, American Institute of Aeronautics and Astronautics, 2024, pp. 1 – 29. https://doi.org/10.2514/6.2024-2677.

[27] Rajpal, D., De Breuker, R., Timmermans, H., Lammen, W., and Torrigiani, F., "Including aeroelastic tailoring in the conceptual design process of a composite strut braced wing," *31st Congress of the International Council of the Aeronautical Sciences, ICAS 2018*, 2018, pp. 1 – 12. URL http://resolver.tudelft.nl/uuid:5c9b55f4-b3b7-4baf-bd38-f143595d7341.

[28] Ferede, E., and Abdalla, M., "Cross-sectional modelling of thin-walled composite beams," *The proceedings of AIAA sciences and technology forum 2014*, edited by R. Braun and J. Evans, American Institute of Aeronautics and Astronautics Inc. (AIAA), United States, 2014, pp. 1–15. https://doi.org/10.2514/6.2014-0163.

[29] Bosschers, J., Montgomerie, B., Brand, A. J., and Rooij, R. P. J. O. M., "Influence of blade rotation on the sectional aerodynamics of rotating blades," *European Rotorcraft Forum (22nd), Brighton, UK*, 1996, pp. 1 – 23. URL http://hdl.handle.net/10921/1380.

[30] Albazzan, M. A., Harik, R., Tatting, B. F., and Gürdal, Z., "Efficient design optimization of nonconventional laminated composites using lamination parameters: A state of the art," *Composite Structures*, Vol. 209, 2019. https://doi.org/10.1016/j.compstruct.2018.10.095.

[31] IJsselmuiden, S. T., Abdalla, M. M., and Gürdal, Z., "Implementation of strength-based failure criteria in the lamination parameter design space," *AIAA Journal*, Vol. 46, 2008, pp. 1826–1834. https://doi.org/10.2514/1.35565, URL https://doi.org/10.2514/1.35565.

[32] Khani, A., Ijsselmuiden, S. T., Abdalla, M. M., and Gürdal, Z., "Design of variable stiffness panels for maximum strength using lamination parameters," *Composites Part B: Engineering*, Vol. 42, 2011. https://doi.org/10.1016/j.compositesb.2010.11.005.

[33] Gudmundsson, S., *General Aviation Aircraft Design*, Butterworth-Heinemann, Boston, Massachusetts, USA, 2014. https://doi.org/10.1016/C2011-0-06824-2.

[34] Pipistrel by Textron eAviation, "Panthera," https://www.pipistrel-aircraft.com/products/panthera/, 2023. accessed on July 18, 2023.

[35] Dorfling, J., and Rokhsaz, K., "Constrained and unconstrained propeller blade optimization," *Journal of Aircraft*, Vol. 52, 2015. https://doi.org/10.2514/1.C032859.

[36] Werter, N. P. M., and De Breuker, R., "A novel dynamic aeroelastic framework for aeroelastic tailoring and structural optimisation," *Composite Structures*, Vol. 158, 2016, pp. 369–386. https://doi.org/10.1016/j.compstruct.2016.09.044.

[37] Agarwal, B. D., Broutman, L. J., and Chandrashekhara, K., *Analysis and Performance of Fiber Composites*, 4th ed., John Wiley & Sons, 2017.

[38] Daniel, I. M., and Ishai, O., *Engineering Mechanics of Composite Materials*, 2nd ed., Oxford University Press, 2006. https://doi.org/10.2514/4.866821.

COPYRIGHT STATEMENT

The authors confirm that they, and their company or organisation, hold copyright on all the original material included in this paper. The authors also confirm that they have obtained permission from the copyright holder of any third-party material included in this paper to publish it as part of their paper. The authors confirm that they give permission, or have obtained permission from the copyright holder of this paper, for the publication and public distribution of this paper as part of the IFASD 2024 proceedings or as individual off-prints from the proceedings.